PROCEEDINGS, Thirty-Ninth Workshop on Geothermal Reservoir Engineering
Stanford University, Stanford, California, February 24-26, 2014
SGP-TR-202

Parallel Simulation of Thermal-Hydrological-Mechanic (THM) Processes in Geothermal Reservoirs

Shihao Wang, Yi Xiong, Philip Winterfeld, Keni Zhang and Yu-Shu Wu

Department of Petroleum Engineering

Colorado School of Mines

1500 Illinois Street,

Golden, CO, 80401, USA

e-mail:shiwang@mines.edu

Keywords: parallel computing, fully coupled THM simulator, EGS reservoir, geomechanics

ABSTRACT

Energy recovery from geothermal reservoirs involves multiple physical processes, including multiphase fluid flow, heat transfer, and rock deformation. To accurately capture these highly nonlinear THM effects, a simulation of this process would require millions of grid blocks with each grid block containing several equations, resulting in a very large number of equations that are expensive to solve. Therefore, parallel computing is absolutely necessary for large scale geothermal reservoir simulations.

In this paper, we discuss a massively-parallel, fully-coupled THM simulator for geothermal reservoir simulation. The simulator is written in Fortran 90 and the governing equations are solved using Integral Finite Difference Method (IFD). Mechanical deformation effects are captured by solving a mean stress equation, derived from the equations governing deformation of porous media. This equation is computationally efficient and accurate enough for reservoir flow applications. The phase behavior of water-air systems are simulated using a dual-phase EOS module. The simulator has an efficient parallel computation scheme using MPI for communication between processors METIS for domain decomposition, and the Aztec package for solving linear systems.

The simulator has been tested on platforms ranging from PCs to clusters.

1. INTRODUCTION

The Enhanced Geothermal Reservoir (EGS) will play a more and more important role in the recovery of geothermal energy. Meanwhile, the geomechanical effects underground have been shown to be crucial to the production. As such, in the geothermal industry, numerical simulators that are capable of capturing the geomechanical effects on a reservoir scale are in demand. Many efforts have been made to develop THM simulators, e.g. Settari and Walters (2001); Settari et al. (2001); Longuemare et al (2002), but very few (if any) fully coupled THM simulators have been developed.

In this paper, we present a fully implicit, fully coupled, parallel THM simulator called TOUGH2-EGS-MP. TOUGH2-EGS-MP is based on the framework of TOUGH2-MP, e.g. Zhang et al (2001, 2008), which is a general-purpose parallel simulator for multi-dimensional fluid and heat flow and implements the Message Passing Interface (MPI), e.g. Message Passing Forum (1994), for communication between processors. The simulator can be run on PCs with multi-core, multi-process hardware and on clusters with distributed memory.

Our TOUGH2-EGS-MP includes a fully-coupled geomechanical module that implements a mean stress equation, developed from linear elastic theory for a thermo-poro-elastic system.

In TOUGH2-EGS-MP, the MINC method (including the dual-porosity, dual-permeability, and multi-porosity models) is used to model fracture-matrix interaction. In our geomechanical module, the multi-porosity extension of the mean stress equation is applied to the MINC method. To capture the geomechanical effects on fluid and heat flow, correlations that describe the dependence of rock porosity and permeability on effective stress are incorporated into the simulator. The key improvements in the rock mechanical module of the simulator include pressure- and temperature- induced hydro-mechanical behavior of fractured and porous media, and the coupled processes of multiphase fluid and heat flow and rock deformation through porous and fractured rock. The results demonstrate that this novel model can be used for field-scale geothermal reservoir simulation with fluid flow and geomechanical effects in porous and fractured media.

This paper is organized as follows. Firstly we will outline the mathematical and numerical model of TOUGH2-EGS-MP, then we will show its parallel framework, and finally we will present two application examples for this simulator.

2. MATHEMATICAL MODEL AND NUMERICAL APPROACH

2.1 Formulation of Fluid and Heat Flow

In TOUGH2-EGS-MP, the governing equations of fluid and heat flow are both in general conservation form, as follows.

$$\frac{dM^{k}}{dt} = \nabla \cdot \vec{F}^{k} + q^{k} \tag{1}$$

in which k refers mass component or heat. In our simulator, k=1 refers to the water component; k=2 refers to the air component; k=3 refers to the heat 'component'.

By integrating the above equation on a representative element volume (REV), we can get the following integrated governing equation

$$\frac{d}{dt}\int_{V_n} M^{k} dV_n = \int_{\Gamma_n} \vec{F}^{k} \cdot \vec{n} d\Gamma_n + \int_{V_n} q^{k} dV_n \tag{2}$$

In the above equation, $\vec{n}$ is the normal vector on the surface Γ_n, pointing inward to the REV.

On the left side of the above equation, the accumulation term of the fluid equation is

$$M^{k} = \phi \sum_{\beta} S_{\beta} \rho_{\beta} X_{\beta}^{k} \tag{3}$$

The accumulation term of heat equation can be written in a similar way as follows

$$M^{\kappa} = (1-\phi)\rho_R C_R T + \phi \sum_{\beta} S_{\beta} \rho_{\beta} u_{\beta} \tag{4}$$

The accumulation of heat contains two terms. The first term $(1-\emptyset)\rho_R C_R T$ is the energy stored by rock while the second term is the energy stored by fluid.

On the right side of Equation(2), the mass flux of liquids consists of advection and diffusion, as shown in Equation(5).

$$\vec{F}^{k} = \vec{F}_{adv}^{k} + \vec{F}_{dis}^{k} \tag{5}$$

The advective flux of a component is the sum over all phases:

$$\vec{F}^{k} = \sum_{\beta} X_{\beta}^{k} \vec{F}_{\beta} \tag{6}$$

where $\vec{F}_{\beta}$ is given by the multiphase version of Darcy's law;

$$\vec{F}_{\beta} = -K \frac{K_{r\beta}\rho_{\beta}}{\mu_{\beta}} \left(\nabla P_{\beta} - \rho_{\beta} g\right) \tag{7}$$

The diffusive mass flux is given by

$$\vec{F}_{dif}^{k} = -\phi \tau_0 \sum_{\beta} \tau_{\beta} \rho_{\beta} d_{\beta}^{k} \nabla X_{\beta}^{k} \tag{8}$$

where the tortuosity, τ_0, is an intrinsic property of rock matrix ,while the tortuosity τ_β is a property of the fluid. d_β^k is the molecular diffusion coefficient for component κ in phase β.

Heat flow occurs by conduction and convection terms, as shown in Equation (9):

$$\vec{F}^{k=3} = -\left[(1-\phi)K_R + \phi \sum_{\beta} S_{\beta} K_{\beta}\right] \nabla T + \sum_{\beta} h_{\beta} \vec{F}_{\beta} \tag{9}$$

where K_R and K_β are thermal conductivity of the rock and the liquid, respectively, and $\vec{F}_{\beta}$ is the liquid flow term from Equation (5).

2.2 Formulation of Geomechanics Module

To couple geomechanical effects, we introduce one more governing equation into the framework of TOUGH2-MP. Recall that the Hooke's law for isothermal elastic materials is as follows

$$\overline{\overline{\tau}} = 2G\,\overline{\overline{\varepsilon}} + \lambda\left(\varepsilon_{xx} + \varepsilon_{yy} + \varepsilon_{zz}\right)\overline{\overline{I}} \tag{10}$$

where $\overline{\overline{\tau}}$ is the stress tensor, $\overline{\overline{\varepsilon}}$ is the strain tensor,and $\overline{\overline{I}}$ is a unit tensor.

TOUGH2-EGS-MP assumes the rock to be a linear thermo-poro-elastic system. By introducing pore pressure and thermal expansion effects, Hooke's law can be extended to thermo-poro-elastic materials, e.g. Jaeger et al. (2007); Winterfeld and Wu (2011):

$$\sigma_{kk} - \left(\alpha P + 3\beta K\left(T - T_{ref}\right)\right) = \lambda\varepsilon_v + 2G\varepsilon_{kk}, k = x, y, z \tag{11}$$

where ε_v is the volumetric strain, as shown in Equation (12)

$$\varepsilon_v = \varepsilon_{xx} + \varepsilon_{yy} + \varepsilon_{zz} \tag{12}$$

We can see from Equation (11) that Lame's constant represents the effects of uniform strain while the shear modulus represent the effects of directional strain.

By summing over the *x, y* and *z* component of Equation (11) and rewriting it in terms of mean stress and volumetric stain, we get the following equation:

$$\sigma_m - \alpha P - 3\beta K\left(T - T_{ref}\right) = \left(\lambda + \frac{2}{3}G\right)\varepsilon_v \tag{13}$$

in which

$$\sigma_m = \frac{\sigma_{xx} + \sigma_{yy} + \sigma_{zz}}{3} \tag{14}$$

is the mean stress.

Recall the thermo-poro-elastic version of Navier's equation

$$\alpha\nabla P + 3\beta K\nabla T + (\lambda + G)\nabla\left(\nabla\cdot\vec{u}\right) + G\nabla^2\vec{u} + \vec{F} = 0 \tag{15}$$

The above Navier's equation has the displacement vector and cross partial derivatives, making it difficult to be solved. We take partial derivative to it with respect to x-component, y-component and z-component respectively and sum up the results, arriving at one single equation

$$\alpha\nabla^2 P + 3\beta K\nabla^2 T + (\lambda + 2G)\nabla^2\left(\nabla\cdot\vec{u}\right) + \nabla\cdot\vec{F} = 0 \tag{16}$$

where *F* is the body force and the divergence equation can be conveniently expressed as the volumetric strain.

$$\nabla\cdot\vec{u} = \varepsilon_v \tag{17}$$

From Equation (11), the volumetric strain can be expressed by mean stress σ_m. By substituting the expression of volumetric strain into Equation (16) and rearranging it, we can get the following equation

$$\frac{3(1-\nu)}{(1+\nu)}\nabla^2\sigma_m + \nabla\cdot\vec{F} = \frac{2(1-2\nu)}{(1+\nu)}\left(\alpha\nabla^2 P + 3\beta K\nabla^2 T\right) \tag{18}$$

The above equation is the governing equation of mechanical simulation in TOUGH2-EGS-MP. This equation is solved in a similar way as that of fluid and heat flow. The only difference is that the coefficients in mechanical equation is weighted based on the distance, instead of flux direction. Such treatment has been tested and has shown sound stability.

Besides porous media, TOUGH2-EGS-MP is also capable of calculating the mechanical response of fractured media. In this simulator, the multiple interacting continua (MINC) approach is extended to simulate facture and matrix interactions with mechanical effect. The

details of MINC can be found in Pruess and Narasimhan (1985) and Wu and Pruess (1988). The governing geomechanical equation of MINC model can be derived from the dual porosity poroelastic Navier equations, e.g. Bai and Roegiers (1994), as

$$\frac{3(1-\nu)}{(1+\nu)}\nabla^2\sigma_m + \nabla\cdot\vec{F} = \frac{2(1-2\nu)}{(1+\nu)}\sum_{i=1}^{N}\left(\alpha_i\nabla^2 P_i + 3\beta_i K\nabla^2 T_i\right) \tag{19}$$

where *i* denotes a certain block of continua and *N* is the total number of blocks in each MINC set.

2.3 Rock Deformation Model

In TOUGH2-EGS-MP, fluid and thermal equations are coupled with geomechanical equation by correlating porosity, permeability, volume, distance and interface area with effective stress.

There have been various permeability-stress and porosity-stress model proposed, e.g. Ostensen et al. (1986); McKee et al. (1988); Davies and Davies (2001); Rutqvist et al. (2002). In TOUGH2-EGS-MP, the above correlations have been included. Users can choose the proper correlation for their specific cases.

Rutqvist et al. (2002) provide the following correlations for porosity and permeability versus effective stress.

$$\phi = \phi_r + (\phi_0 - \phi_r)e^{-\alpha\sigma'} \qquad K = K_0 e^{c(\phi/\phi_0 - 1)} \tag{20}$$

where $\emptyset_0$ is the porosity under zero effective stress and $\emptyset_r$ is the porosity under high effective stress. α is a constant parameter. K_0 is the permeability under $\emptyset_0$ and c is a constant.

The geomechanical effects on fractures are captured by the aperture change. The following is the correlation between fracture aperture and effective stress.

$$b_i = b_{i0} + \Delta b_i\left(e^{-d\sigma'} - e^{-d\sigma'_0}\right) \tag{21}$$

in which b_{i0} is the 'initial' aperture under initial stress σ'_{i0}.

The porosity and permeability of fracture are correlated with aperture change as

$$\phi = \phi_0\frac{b_1 + b_2 + b_3}{b_{1,0} + b_{2,0} + b_{3,0}} \tag{22}$$

$$K_i = K_{i,0}\frac{b_j^3 + b_k^3}{b_{j,0}^3 + b_{k,0}^3} \tag{23}$$

For both fracture and matrix blocks, as porosity and permeability change, capillary pressure also changes, described by Equation (24).

$$P_c = P_{c0}\frac{\sqrt{(K/\phi)_0}}{\sqrt{(K/\phi)}} \tag{24}$$

The volumetric strain changes the volume of a certain block as follows.

$$V = V_0(1-\varepsilon_V) \tag{25}$$

2.4 Numerical Approach

TOUGH2-EGS-MP uses Integrated Finite Difference (IFD) method to solve the above governing equations, e.g. Narasimhan and Witherspoon (1976); Celia et al. (1990). Using the IFD method, the Equation (2) is discretized as :

$$\frac{\left(V^{i+1}M^{k,i+1} - V^{i}M^{k,i}\right)}{\Delta t} = \sum_m A_{nm}F^{k}_{nm} + q^{k} \tag{26}$$

In the above equation, *i* denotes a certain time step, m denotes a certain connection between two neighboring blocks, and *n* denotes a certain weighting scheme, namely harmonic weighting. The above nonlinear equations are solved by the Newton-Raphson method.

A detailed description of IFD method and the numerical approach used in TOUGH2-EGS-MP can be found in the work of Fakcharoenphol and Wu. (2011) and Winterfeld et al. (2013).

3 PARALLEL FRAMEWORK

TOUGH2-EGS-MP is based on MPICH2, e.g. Gropp (2002). The parallel framework of TOUGH2-EGS-MP consists of two parts: the parallel preprocessing part and the parallel simulation part.

3.1 Parallel Preprocessing

TOUGH2-EGS-MP adopts domain decomposition approach to solve the fully-coupled nonlinear system, in which each processor is assigned with a subdomain of the whole reservoir. As such, a parallel preprocessing module is needed to process input data and distribute work.

In TOUGH2-EGS-MP, a master-slave framework is used in which a randomly chosen processor, called the master processor, reads the input file, sets up the global mesh, calls METIS to do graph partition, and distributes local versions of information to every processor. From the master processor, the other processors, named slave processors, receives their local version of connection list, pointers of the Jacobian matrix, and initial conditions. In this process, the master processor has to store some global versions of arrays, such as the permeability of all elements, which may take huge amounts of memory. To optimize memory usage, the above operations are conducted one at a time so that the master processor will not store many global arrays at the same time. A detailed flowchart of this preprocessing framework is shown in Figure 1.

The advantage of the master-slave framework is that it is simple and easy to implement. A drawback of this framework is that it is not scalable. But as the CPU time spent in preprocessing is only a small portion of the total simulation time, the loss of scalability is negligible in most cases, as shown in the application section of this paper.

To partition the whole reservoir domain, TOUGH2-EGS-MP uses the METIS package, which is a widely used graph partitioning tool. A detailed technique description of METIS can be found in the work of Karypis and Kumar (1995). METIS requires the graph to be stored in the adjacency list format. METIS partitions the reservoir into several overlapping subdomains. The inner part of a subdomain is called the UPDATE part, while the border of the subdomain is called the EXTERNAL part. As such, the EXTERNAL part of a certain subdomain is located in the UPDATE part of one of its neighboring subdomains. In this paper, we call such elements the overlapping elements.

3.2 Parallel Simulation

For the parallel simulation part of the framework, in each nonlinear iteration step each processor builds its local part (UPDATE) of the Jacobian matrix and residual array. After the Jacobian matrix is built, the AZTEC package, e.g.Tuminaro et al. (1999), the iterative linear solver, is called simultaneously by all the processes to solve the linear system, e.g. Wu et al. (2002).

AZETEC gives back the increments of the primary variables of the UPDATE part to its processor. After each iteration, increments of the primary variables of the overlapping elements are exchanged between neighboring processors and each processor updates the secondary variables on both UPDATE and EXTERNAL parts of its subdomain. As such, the secondary variables on the border are calculated repeatedly by neighboring processes. The purpose of such treatment is to reduce the amount of communication among processes, which is far more expensive than computation.

To avoid processor conflicts, all the job's output is carried out by the master processor. As such, after each time step, all processors send their information back to the master process, in order to generate printout file.

In summary, input/output and distribution of work is carried out by the master processor, while most time-consuming work, including assembling the Jacobian matrix and solving linear system, is done in parallel by all processors. A detailed parallel simulation framechart is shown in Figure 2.

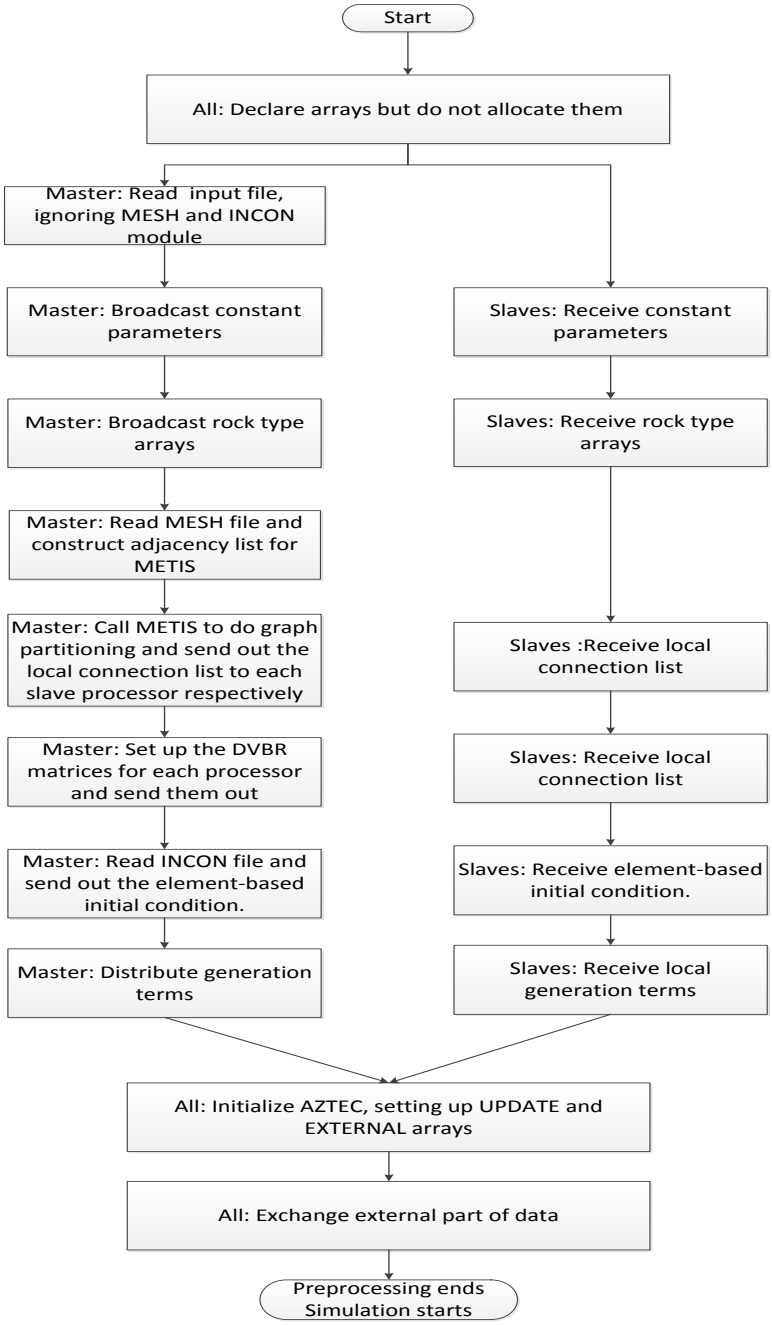

Figure 1: Flowchart of parallel preprocessing part of the simulator.

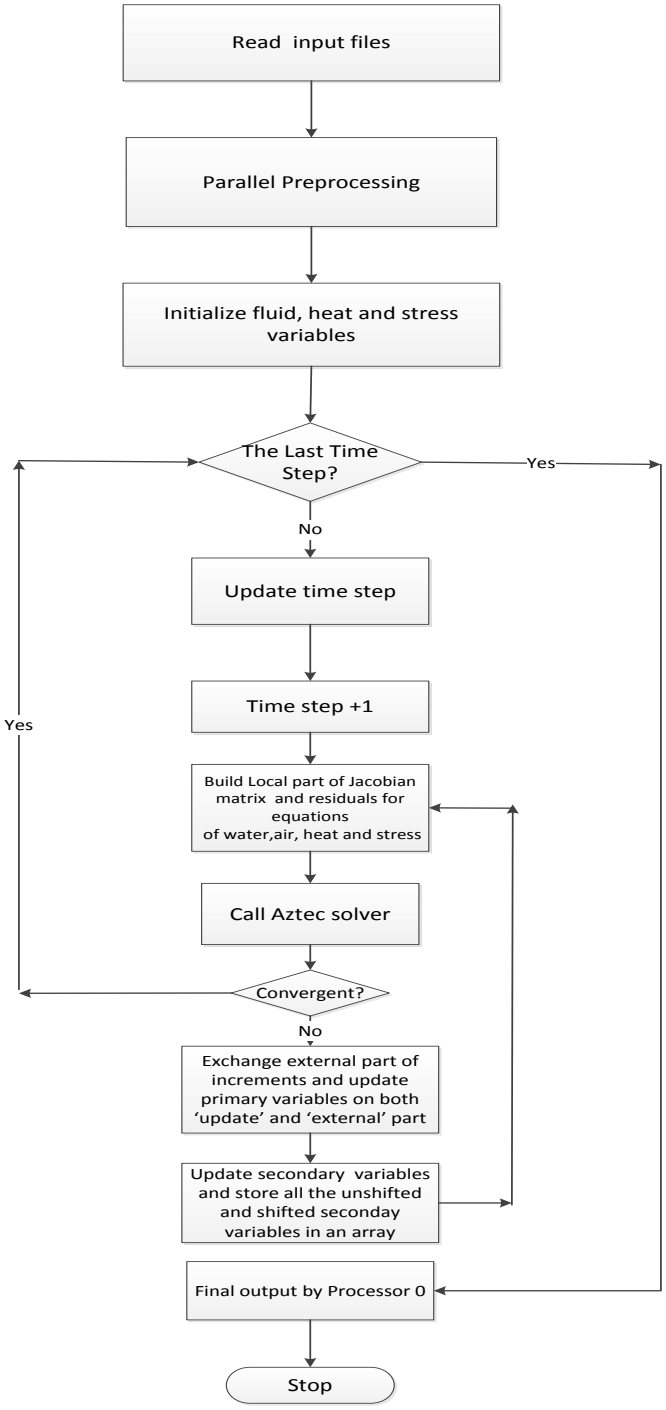

Figure 2: Flow chart of the whole simulator. The details of the parallel preprocessing step is shown in Figure 1.

4 APPLICATION AND DISCUSSION

In this section, we present two application examples to show the parallel performance and computational efficiency of our simulator.

4.1 2-Dimensional Compaction with Mandel-Cryer Effect

In this example, we use our simulator to solve the two dimensional compaction problem. Given a piece of saturated poroelastic material, a constant compressive force is applied on the top, compressing the material and causing the pore pressure inside to increase. Afterwards, the material is allowed to drain on the lateral direction. The drainage occurs on the edges and leads to the decrease of pore pressure there, causing some additional load to be transferred to the center of the material. The pore pressure in the center will continue

to increase until it reaches a maximum and then declines. This effect was firstly studied by Mandel (1953) and is called the Mandel-Cryer effect. Later, Abousleiman and et al.(1996) presented an analytical solution to this problem. Figure 3 shows its configuration.

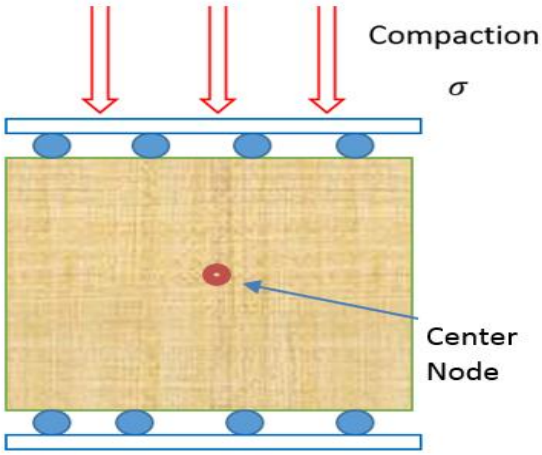

Figure 3 Problem description of 2-dimensional compaction.

In this paper, we study the Mandel-Cryer effects under different permeability conditions. Case #1 has a higher permeability and case #2 has a lower permeability.

Table 1 Input parameters for 2-D compaction cases.

Properties	Values	Units
Permeability of case #1	$Kx=Kz=3.0*10^{-13}$	m^2
Permeability of case #2	$Kx=Kz=1.0*10^{-15}$	m^2
Porosity	0.15	dimensionless
Young's modulus	15.0	GPa
Poisson's ratio	0.3	dimensionless
Biot's coefficient	1.0	dimensionless
Water viscosity	0.001	Pa·S

For both cases, the material is discretized into 20*24=480 grid blocks with uniform size. The problem is solved by a PC work station. The PC has an Intel Core i7 processor with 16 processes and 32Giba bytes of memory. The simulation is run by 4, 8 and 16 processes. The partitioned graph of the case of 8 processes is shown in Figure 4, from which we can see that METIS roughly partitions the graph evenly.

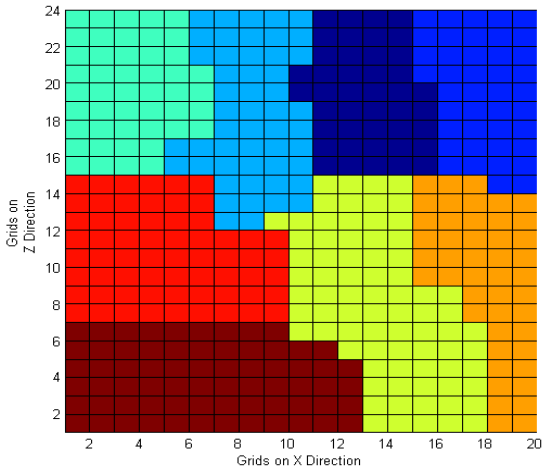

Figure 4 Partitioned graph of the 2-D compaction case. Different colors refer to the 8 different subdomains.

Table 1 shows the input parameters for two cases. Both cases are solved in two steps. In the first step, we apply the compaction force on the top of the material. We run this simulation for a sufficient long time to reach an equilibrium state for the material. In the second step, we remove the compressive stress and let the water inside the material drain from its two sides. We then plot the pore pressure of the center grid block versus time.

The difference of the results between any two cases with different number of processes is always less than 0.1%, so we only present the results with 8 processes, shown in Figure 5. As the permeability of the material increases, the fluid drains more quickly and thus the peak of pore pressure comes earlier. From this comparison, we can draw the conclusion that a reservoir with higher permeability reacts faster that one with lower permeability.

Figure 5 also shows the comparison between TOUGH2-EGS-MP's results and the analytical solution. We find out that our numerical results match well with the analytical solution, verifying the accuracy of our simulator.

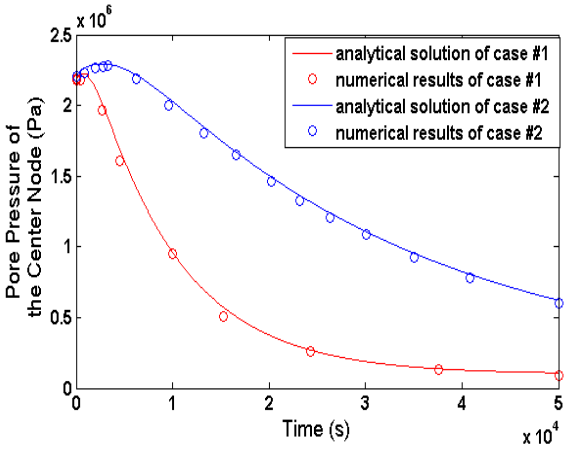

Figure 5 Comparison between numerical results and numerical results (8 processes) of 2-dimensional compaction. Red line refers to higher permeability case, while blue line refers to lower permeability case.

4.2 Field-Scale Case with Over a Million of Grid Blocks

We present a large reservoir grid to show the numerical performance of our simulator. The reservoir is a 5km*5km*2.5km domain, fully saturated with water phase. There is a producing well in the center, penetrating 1km in Z direction. Figure 6 shows the mesh for the simulation case. The mesh is distributed logarithmically in the X and Y directions starting from the center, which is the simulation area of interest. There are a total of 129*129*100 = 1,664,100 grid blocks in this simulation. We set the initial pore pressure to be 5Mpa with constant pressure-stress boundary condition and run the simulation for an efficient long time to get to an equilibrium state, which is then used as the initial condition for the next step of this problem. We then run the simulation for 4 years. As TOUGH2-EGS-MP has already been verified in Section 4.1, we only show the numerical performance of the simulator.

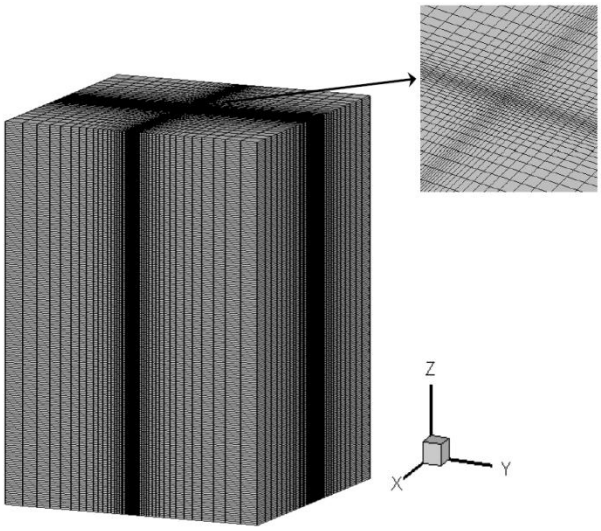

Figure 6 Problem description of the large reservoir case. The small picture on the top right is a close look of the area of interest.

The problem is run on a LINUX cluster with 32 computational nodes and 512 processes. Table 2 summarizes the numerical performance, including the number of processes, the total CPU time, and speedup factors. As TOUGH2-EGS-MP cannot be run with single process, the minimum number of processes we use is 2. As shown in Table 2, the speedup at low number of processes is very close to linear. As such, we assume a linear speedup from the 2-process case. We then multiply the CPU time of 2-process case by 2 to estimate the CPU time of 1-process serial case, as shown in the first row of Table 2. From Table 2, the speedup of the case with 256 processes is 112.97.

Figure 7 gives the plot of speedup versus number of processes. According to Figure 7, the first several points indicate a linear speedup. Such trend is slowed as the number of process continues to increase. The reasons for this are as follows. On the one hand, as shown in Table 2, the time spent in the parallel preprocessing part is almost the same for cases with different number of processes. This is due to the lack of scalability of the master-slave framework used in this simulator. On the other hand, according to Table 3, as the whole reservoir is partitioned into more subdomains, more elements are exposed by the partition and become the elements on the borders. As such, the fraction of border (EXTERNAL) elements increases, resulting in more communication and more overlap of work between neighboring subdomains. Therefore, as number of processes increases, the more time is spent on pre-processing relatively and more communication is involved, so the speedup has to be slowed down to some extent.

In general, although several factors may limit the maximum speedup, the speedup is more than 100 times and the total CPU time has been decreased from more than one day (36 hrs) to less than one hour (1669 s) for one to 256 processes. Therefore, TOUGH2-EGS-MP can greatly speed up the numerical analysis of large reservoirs.

Table 2 Summary of Computation Configuration and Performance

No. of Processes	Total CPU Time (s)	Pre-processing Time (s)	Speedup	Ideal Speedup
1	**188642.86**			
2	94321.4	60.42	2	2
4	48871.19	64.14	3.86	4
8	25876.93	64.35	7.29	8
16	14067.32	64.23	13.41	16
32	7421.03	64.16	25.42	32
64	4701.96	67.53	40.12	64
128	2697.42	69.35	69.92	128
256	**1669.85**	**73.42**	112.97	256

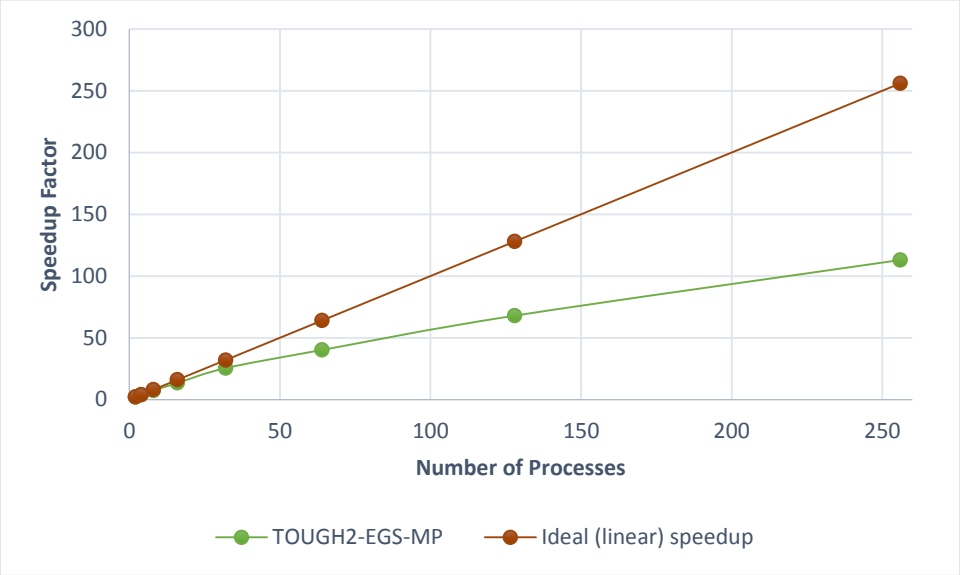

Figure 7 Comparison of the parallel speedup between TOUGH2-EGS-MP and ideal performance

Table 3 Summary of the number of inner (UPDATE) and border (EXTERNAL) elements per process for each case

No. of Processors	Average No. of Inner Elements	Average No. of Border Elements	Inner-Border Ratio
16	104000	3190	32.6
32	52000	2023	25.7
64	26000	1333	19.5
128	13000	1008	12.9
256	6500	878	7.4

5 CONCLUSIONS

We have presented a massively parallel, fully coupled THM simulator TOUGH2-EGS-MP with two application examples.

In the first application case, the accuracy of the simulator is verified. Our results match well with the analytical solution of the 2D compaction problem with Mandel-Cryer effect. It has be shown that the mechanical simulation module in this simulator can accurately capture the stress field change and rock deformation.

In the second case, the improved performance of the parallel simulator is demonstrated. A case of large reservoir simulation with more than 1 million grid blocks is tested. Typically it is not practical to use serial simulators to simulate such a large case with fully coupled THM equations. However, our results show that using our simulator, the computational time can be reduced by 1~2 magnitude, with a maximum speedup factor of more than 100.

Overall, TOUGH2-EGS-MP is able to simulate coupled flow and rock deformation. Meanwhile, this simulator is capable of conducting field-scale simulations under its parallel framework. As such, it can be applied to large stress-sensible EGS reservoirs for analyzing multiphase fluid and heat flow, and rock deformation.

ACKNOWLEDGEMENT

The work presented in this paper is supported by the U.S. Department of Energy under Contract No. DE-EE0002762, “Development of Advanced Thermal-Hydrological-Mechanical-Chemical (THMC) Modeling Capabilities for Enhanced Geothermal Systems”. Special thanks are due to Energy Modeling Group (EMG) of Colorado School of Mines. Foundation CMG and Lawrence Berkeley National Laboratory (LBNL).

NOMENCLATURE

k = a certain component

β = a certain phase

K = absolute permeability. m^2

g = gravity terms, m/sec^2

P = pore pressure, Pa

S = phase saturation,

K_r = relative permeability

X = mass component

M = accumulation term

F = flux term

q = generation term, kg/s

u = phase specific internal energy, J/kg

T = temperature, K

S = phase saturation, dimension less

$\emptyset$ = porosity, dimension less

ρ = density, kg/m^3

V = volume, m^3

σ' = effective stress, Pa

σ_m = mean stress, Pa

α = Biot's coefficient, dimension less

b_i = fracture aperture on the *i* direction, m

A = area of a connection, m^2

K_R = formation heat conductivity, W/m ºC

K_β = liquid heat conductivity, W/m ºC

Pc = capillary pressure, Pa

Δt = length of time step, s

$\vec{u}$ = displacement vector, m

h = enthalpy, J

$\boldsymbol{\lambda}$ = Lame's coefficient, Pa

G = shear modulus, Pa

REFERENCES

Abousleiman, Y., A.D. Cheng, L. Cui, E. Detournay, and J.C. Roegiers. (1996), "Mandel's problem revisited." *Geotechnique*, 46(2), 187-195.

Bai, M, and J.C. Roegiers. (1994), "Fluid flow and heat flow in deformable fractured porous media." *International journal of engineering science* **32**, no. 10: 1615-1633.

Celia, M. A., E.T. Bouloutas, and R.T. Zarba. (1990), "A general mass-conservative numerical solution for the unsaturated flow equation." *Water resources research*, 26(7), 1483-1496.

Davies, J. P., and D. K. Davies. (2001), "Stress-dependent permeability: characterization and modeling." *SPE Journal*, **6**.2: 224-235.

Gropp, W. (2002), "MPICH2: A new start for MPI implementations." In *Recent Advances in Parallel Virtual Machine and Message Passing Interfac*e (pp. 7-7). Springer Berlin Heidelberg.

Jaeger, J. C., N. G. W. Cook, and R. W. Zimmerman. (2007), "*Fundamentals of rock mechanics*." Blackwell Fourth edition.

Karypis, G. and V. Kumar. (1995), Metis-unstructured graph partitioning and sparse matrix ordering system, version 2.0.

Longuemare, P., M. Mainguy, P. Lemonnier, A. Onaisi, C. Gérard, and N. Koutsabeloulis. (2002), "Geomechanics in reservoir simulation: overview of coupling methods and field case study." *Oil & Gas Science and Technology*,57(5), 471-483.

Mandel, J. (1953), "Consolidation Des Sols (Étude Mathématique).." *Geotechnique*, 3(7), 287-299.

McKee, C. R., A. C. Bumb, and R. A. Koenig. (1988), "Stress-dependent permeability and porosity of coal and other geologic formations." *SPE formation evaluation*, **3**.1: 81-91.

Message Passing Forum.(1994), "A Message-Passing Interface Standard." *International Journal of Supercomputing Applications and High performance Computing*, 8(3-4).

Narasimhan, T. N., and P. A. Witherspoon. (1976), "An integrated finite difference method for analyzing fluid flow in porous media." *Water Resources Research*, **12**.1: 57-64.

Ostensen, R. W. (1986), "The effect of stress-dependent permeability on gas production and well testing." *SPE Formation Evaluation*, **1**.3: 227-235.

Fakcharoenphol, P. and Y. S. Wu. (2011), "A coupled flow-geomechanics model for fluid and heat flow for enhanced geothermal reservoirs." In *45th US Rock Mechanics/Geomechanics Symposium*. American Rock Mechanics Association.

Pruess, K. and T.N. Narasimhan. (1985), "A Practical Method for Modeling Fluid and Heat Flow in Fractured Porous Media." *Soc. Pet. Eng. J.*, **25**, 14-26.

Rutqvist, J., Y. S. Wu, C. F. Tsang, and G. Bodvarsson. (2002), "A modeling approach for analysis of coupled multiphase fluid flow, heat transfer, and deformation in fractured porous rock." *International Journal of Rock Mechanics and Mining Sciences* **39**, no. 4: 429-442.

Settari, A., and D. A. Walters. (2001), "Advances in coupled geomechanical and reservoir modeling with applications to reservoir compaction." *Spe Journal*, 6(03), 334-342.

Settari, A., Walters, D. A., and G. A. Behie (2001). "Use of coupled reservoir and geomechanical modelling for integrated reservoir analysis and management." *Journal of Canadian Petroleum Technology*, 40(12).

Tuminaro, R. S., M. Heroux, S. A. Hutchinson, and J. N. Shadid. (1999), "Official Aztec User's Guide."

Winterfeld, P. H., and Y. S. Wu. (2011), "Parallel simulation of CO2 sequestration with rock deformation in saline aquifers. In *SPE Reservoir Simulation Symposium*. Society of Petroleum Engineers.

Winterfeld, P. H., Y. S. Wu, R. Zhang, P. Fakcharoenphol, and Y. Xiong. (2013), "Coupled geomechanical and reactive geochemical model for fluid and heat flow: application for enhanced geothermal reservoir." In *SPE Reservoir Characterization and Simulation Conference and Exhibition*. Society of Petroleum Engineers.

Wu, Y. S., and K. Pruess. (1988), "A multiple-porosity method for simulation of naturally fractured petroleum reservoirs." *SPE (Society of Petroleum Engineers) Reserv. Eng*; (United States), 3(1).

Wu, Y. S., K. Zhang, C. Ding, K. Pruess, E. Elmroth, and G. S. Bodvarsson. (2002). "An efficient parallel-computing method for modeling nonisothermal multiphase flow and multicomponent transport in porous and fractured media." *Advances in Water Resources*, 25(3), 243-261.

Zhang, K. N., Wu, Y. S., Ding, C., Pruess, K., and Elmroth, E. (2001), "Parallel computing techniques for large-scale reservoir simulation of multi-component and multiphase fluid flow." In *SPE Reservoir Simulation Symposium*. Society of Petroleum Engineers.

Zhang, K., Wu, Y. S., and K. Pruess (2008), "User's guide for TOUGH2-MP: a massively parallel version of the TOUGH2 code. " *Report LBNL-315E*, Lawrence Berkeley National Laboratory, Berkeley, CA.